

# CHAPTER 110

## Wave Energy Dissipation on and in Rubble Mound Structures

M. Muttray<sup>1)</sup>, H. Oumeraci<sup>2)</sup>, C. Zimmermann<sup>3)</sup>, H. W. Partenscky<sup>4)</sup>  
University of Hannover, SFB 205, Franzius-Institut, Hannover/ Germany

### **Abstract**

The results of large-scale model tests are presented on the wave energy dissipation in the various layers of an Accropode armoured mound breakwater and on the interaction between external and internal wave motion. An attempt is also made to describe the "discontinuity" of the waterline at the boundary between layers of different porous materials. Wave reflection coefficients of the structure as well as dissipation and transmission coefficients through the different layers are evaluated as a function of the incident wave parameters.

### **Introduction**

In a previous paper it was shown that a) an improvement of the evaluation of the reflected wave energy is required as it represents an important portion of the incident wave energy, b) most of the incident wave energy is dissipated within the armour and underlayer and that a better description of the wave-induced flow in these regions is needed and (c) a good knowledge of the external flow and its interaction with the internal flow is needed as this represents a prerequisite for the development of a mathematical/numerical model for the internal flow field (OUMERACI & PARTENSCKY, 1990).

In this respect, further large-scale model tests have been performed in the Large Wave Flume (GWK), Hannover. The main objectives of these tests consist in the study of a) the interaction of the external and internal wave motion and b) the energy dissipation within the various layers of the structure, especially that dissipated in the first layers (high turbulent flow).

The present paper principally intends to present and discuss the first results of these tests which will certainly have some implications for the simulation of the wave-induced flow on and in rubble mound structures by using small-scale model tests and mathematical/numerical models (WIBBELER & OUMERACI, 1992).

### **Experimental Set-up and Test Conditions**

The experimental set-up in the Large Wave Flume (GWK) of Hannover is given in Fig. 1, showing

---

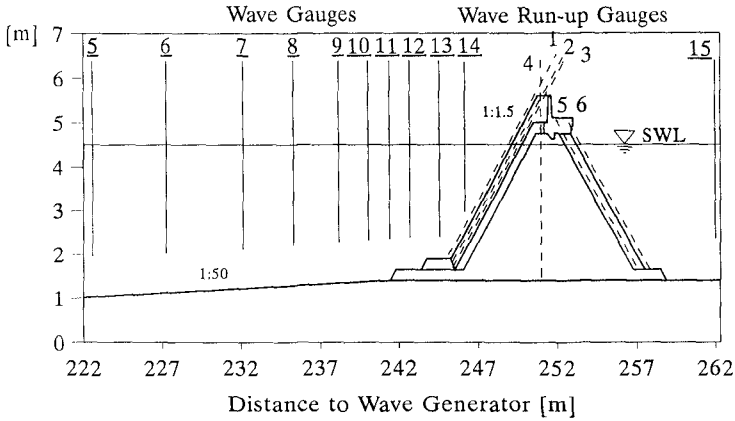
<sup>1)</sup> Dipl.-Ing., Research Engineer, SFB 205

<sup>2)</sup> Dr.-Ing., Senior Researcher, SFB 205

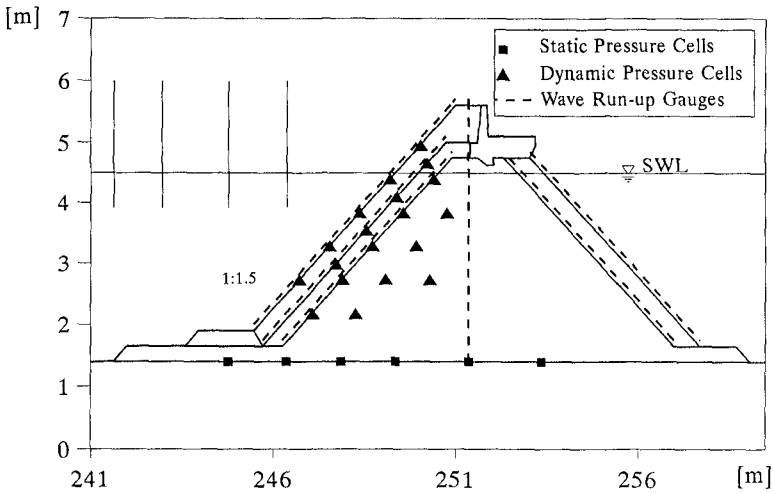
<sup>3)</sup> Prof. Dr.-Ing., Managing Director Franzius-Institut

<sup>4)</sup> Prof. Dr.-Ing. Dr.-Phys., formerly Managing Director Franzius-Institut

- a) the cross-section of the model with the position of the pressure and "wave run up" gauges on and within the structure and
- b) the location of the wave gauges in front of and behind the structure.



a) Location of Wave Gauges



b) Location of Pressure Cells and 'Wave Run-up' Gauges

FIG. 1-EXPERIMENTAL SET-UP IN THE LARGE WAVE FLUME (GWK)

Four wave gauges in deeper water are used to determine the incident and reflected wave by using the 3-wave-gauge-procedure (MANSARD & FUNKE, 1987). Ten wave gauges on the foreshore are installed to analyse the wave field in front of the structure. The positions of these gauges are shown in Fig. 1a.

A cross section of the breakwater model with the position of the pressure cells and the wave run-up gauges is shown in Fig. 1b. Six wave run-up gauges and six static pressure cells were used to record the surface elevation on and in the structure. In order to measure the pressure variation in the most turbulent zone, 19 dynamic pressure cells were placed within the first layers of the structure.

The mean grain size of the core material (crushed stones) is  $d_{50}=4\text{cm}$  and the uniformity coefficient  $U=d_{60}/d_{10}=2.2$ . The underlayer is made of crushed stone of 0.5-5.0 kg ( $d_{50}=12\text{ cm}$ ), whereas the armour is composed of a single layer of 40kg Accropodes.

Regular waves with heights  $H=0.20\text{-}1.80\text{m}$  and periods  $T=3.0\text{-}12.0\text{s}$ , and irregular waves (TMA Spectra) with significant heights  $H_s=0.20\text{-}1.20\text{ m}$  and peak periods  $T_p=3.0\text{-}12.0\text{s}$  were used. Most of the wave spectra had a groupiness factor  $GF=0.77$ . However, some tests were carried out with groupiness factors  $GF=0.6\text{-}0.9$  in order to examine the effect of the groupiness factor on the results. The water depths in the wave flume was varied from  $d=4.20\text{m}$  to  $d=4.80\text{m}$ .

In the results presented below only non-overtopping test conditions are considered, i.e. regular waves with  $H=0.20\text{-}0.85\text{m}$  and  $T=3.0\text{-}12.0\text{s}$  and irregular waves with  $H_s=0.20\text{-}0.70\text{m}$  and  $T_p=3.0\text{-}12.0\text{s}$

For the conditions tested, REYNOLDS numbers (related to the grain size of the core material) in the range of  $10^5$  to  $10^6$  are expected within the core material; i.e. no scale effects due to the dissimilarity of viscous forces will occur.

## Discussion of Experimental Results

### **General Considerations**

As already mentioned, only tests with non-overtopping wave conditions are considered. In addition, no wave breaking occurs in front of the structure. In this case, the incident wave energy is splitted up into reflected, dissipated and transmitted wave energy.

$$E_i = E_r + E_d + E_t \quad (1)$$

The wave reflection coefficient ( $K_r$ ), the dissipation coefficient ( $K_d$ ) and the transmission coefficient ( $K_t$ ) are correlated by the relationship:

$$K_r^2 + K_d^2 + K_t^2 = 1 \quad (2)$$

$$\text{with } K_r = \sqrt{\frac{E_r}{E_i}}, \quad K_d = \sqrt{\frac{E_d}{E_i}} \quad \text{and} \quad K_t = \sqrt{\frac{E_t}{E_i}}$$

and where  $E_i$ ,  $E_r$ ,  $E_d$  and  $E_t$  are the incident, reflected, dissipated and transmitted (through the structure) wave energy components, respectively. Each of these energy components is considered to be expressed by the corresponding wave height squared ( $E_i \sim H_i^2$ ). The total dissipated wave energy  $E_d$  may be divided into the dissipated energy component on and in the armour layer ( $E_{da}$ ), on and in the underlayer ( $E_{du}$ ) and in the core ( $E_{dc}$ ),

$$E_d = E_{da} + E_{du} + E_{dc} \tag{3}$$

so that the following relationship for the corresponding local dissipation coefficients will result:

$$K_{da}^2 + K_{du}^2 + K_{dc}^2 = 1 \tag{4}$$

with  $K_{da} = \sqrt{\frac{E_{da}}{E_d}}$  ,  $K_{du} = \sqrt{\frac{E_{du}}{E_d}}$  and  $K_{dc} = \sqrt{\frac{E_{dc}}{E_d}}$

Eqs. (2) & (4) build the principal basis for the analysis and discussion of the experimental results . The porous structure and its geometry being given, the quantities involved in Eqs. (2) & (4) are determined by the prevailing water depth and incident wave parameters. The relative water depth ( $d/L$ ) and the wave steepness are expected to be the most relevant influencing parameters, since they strongly affect the shapes and kinematics of the waves at the structure. Since the latter are commonly described by the surf similarity parameter, its application to characterise the prevailing breaker types in the case of relatively high reflection coefficients and high velocity currents during the wave run down process on steep slopes is briefly discussed.

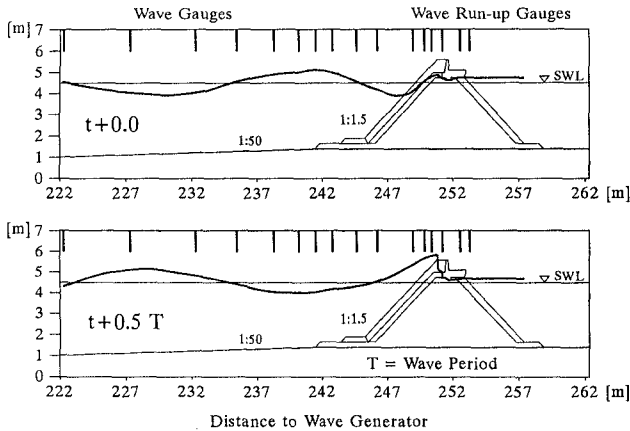


FIG.2 WAVE MOTION OUTSIDE AND INSIDE THE BREAKWATER

### Interaction Between External and Internal Wave Motion

Based on the wave motion simultaneously recorded at wave gauges 5-14 (Fig.1a) and "run-up gauges" 1-6 (Fig.1b), a detailed description of the external wave motion and the wave motion in the different layers of the breakwater is given, illustrating how the internal and external flow field influence each other.

The wave motion in front of the structure is described by using video records and the wave gauges located in that area. These records are intended to be used for the description of the breaker types, the volume and the velocity of the waves.

An example of the temporal variation of the surface elevation outside and inside the breakwater is shown in Fig.2 for an incident wave period  $T=4.5s$ , a wave height  $H=0.82m$  and a water depth  $d=4.50 m$ .

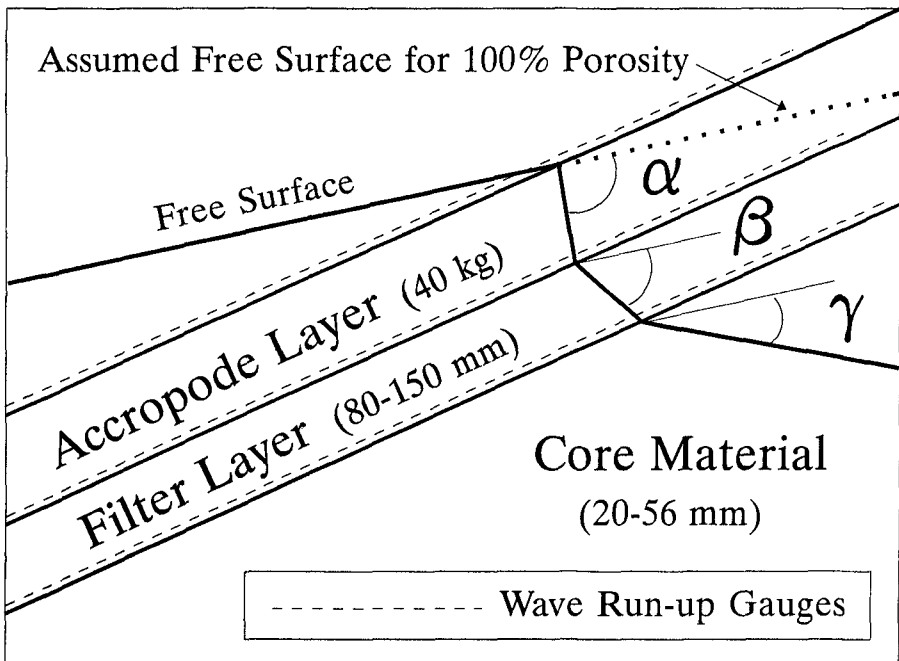


FIG.3 PRINCIPLE SKETCH FOR DISCONTINUITY ANALYSIS

An attempt is made below to partially describe the "discontinuity" of the waterline at the boundary between two layers of different porous materials. A

discontinuity of the waterline is generally expected at the boundary of two layers with different hydraulic resistance. Even by using the wave run-up gauges as shown in Fig.1b this discontinuity can not be described accurately. Despite the limitations resulting from this measurement procedure, an attempt is made to get an approximate description of the waterline within the first layers during the wave run-up and run-down process. For this purpose three angles  $\alpha$ ,  $\beta$ ,  $\gamma$  are defined in Fig.3. The definition of these angles is based on the assumption, that the free surface at the outer slope would continue to be represented by a *straight line* if the first layers had 100% porosity and no hydraulic resistance. It is therefore suggested that the deviation of the waterline from its straight course is caused by the relative difference in hydraulic resistance between two successive layers. Angles  $\alpha$ ,  $\beta$  and  $\gamma$  describe this deviation at the boundaries between the outer slope (Accropode layer), filter layer and core material, respectively. It is suggested that the analysis of the relationship between these angles and the wave parameters should lead to an approximate description of the discontinuity of the waterline at the boundary between two adjacent layers.

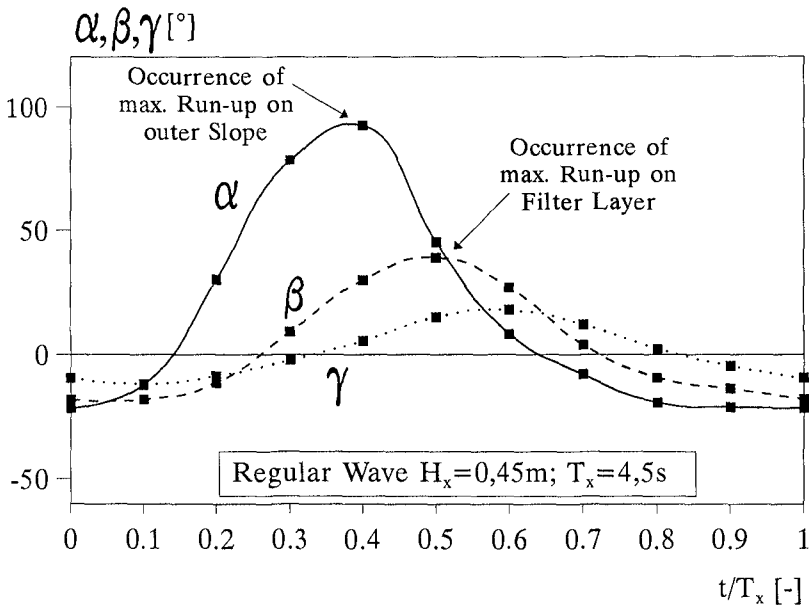


FIG.4 TEMPORAL RELATIVE VARIATION OF ANGELS  $\alpha$ ,  $\beta$  AND  $\gamma$

The temporal relative variation of the three angles  $\alpha$ ,  $\beta$  and  $\gamma$  during one wave period starting with the wave run-down at its lowest elevation is shown in Fig.4. Angle  $\alpha$  reaches a maximum at the highest run-up on the armour layer,  $\beta$  and  $\gamma$  at the highest run-up on the underlayer and on the core material, respectively. It is seen

that the maximum value of angle  $\gamma$  occurs later than that of angle  $\beta$  and that the occurrence of the maximum value of angle  $\beta$  is much more delayed as compared to that of angle  $\alpha$ .

In addition, it is found that the variation of  $\alpha$ ,  $\beta$  and  $\gamma$  strongly depends on the wave height. This is shown by Fig.5 illustrating the increase of angle  $\alpha$  with incident regular wave heights. This increase was expected, since angle  $\alpha$  was supposed to describe the hydraulic resistance of the Accropode layer and thus represents a measure of the hydraulic loss (dissipated energy). The same trend is also found for angles  $\beta$  and  $\gamma$ , but the effect of the wave height is less pronounced than for angle  $\alpha$ .

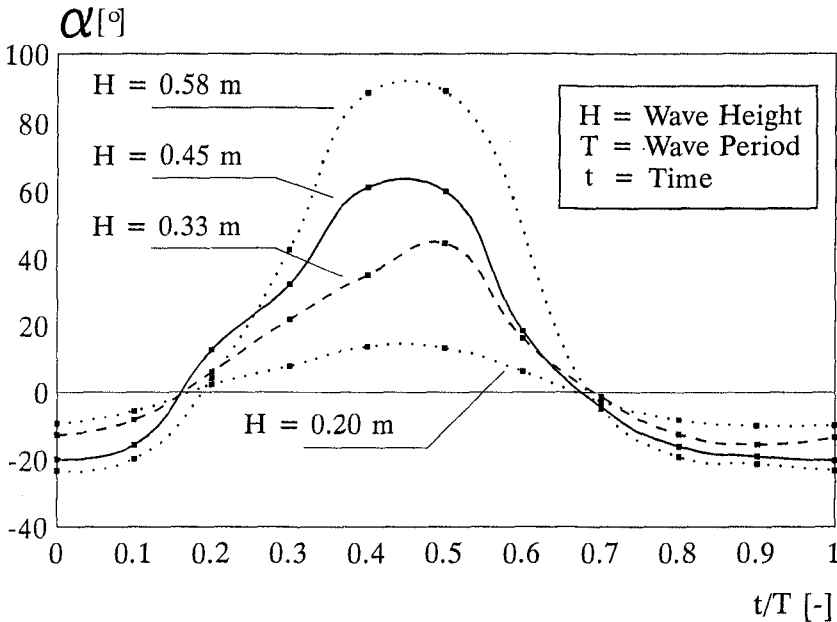


FIG.5 EFFECT OF WAVE HEIGHTS ON ANGLE  $\alpha$

### Wave Reflection Coefficients

The separation of induced and reflected wave components from the measured partial standing wave system taking place in front of a sloping porous structure still represents one of the most difficult tasks in hydraulic model tests. In Fig.6, the partial standing wave in front of the structure is shown for different wave conditions.

Due to non-linearities, cross-wave phenomena and measurement inaccuracy, simultaneous wave records at more than two different locations in the wave flume (in the direction of wave propagation) is required. Therefore, four wave gauges with different spacing in front of the structure are used. Depending on the prevailing wave periods, three wave probes are optimally selected for the reflection analysis. Details of the reflection analysis used in this study are given by MANSARD & FUNKE (1987).

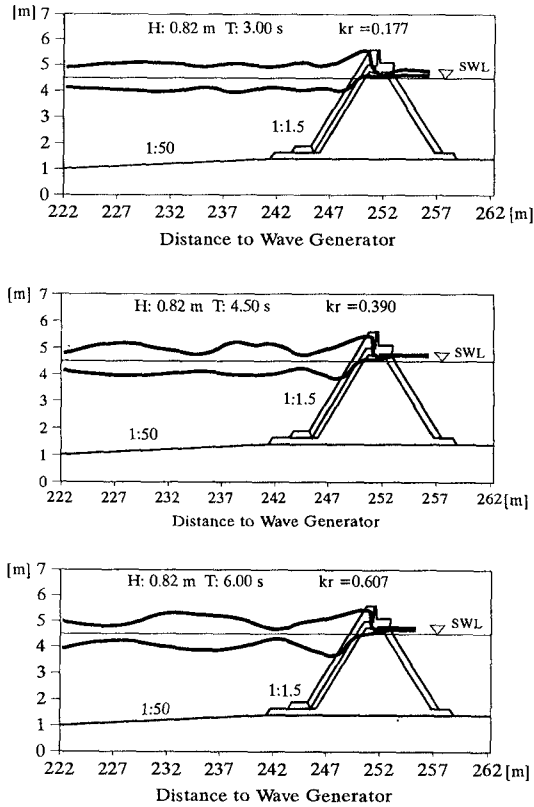


FIG. 6 PARTIAL STANDING WAVE IN FRONT OF THE BREAKWATER

Reflection coefficients  $K_r$  are determined as a function of relative depth  $kd$  ( $k=2\pi/L$ ), wave period  $T$ , wave height  $H$ , wave steepness  $H/L$  and onshore surf similarity parameter  $\xi$  ( $= \tan \alpha / (H/L)^{0.5}$ ).

Fig.7 shows the relationship between wave period and reflection coefficient  $K_r$ , which is stronger for irregular waves than for monochromatic waves. The wave periods on the x-axis refer to prototype conditions in which  $H_s=1.60-6.60\text{m}$  and  $H/L=.005-0.063$  were considered for this figure. For large values of the wave period, reflection coefficients of more than 50% may result and the reflection coefficient for regular waves is about up to 10% larger than for irregular waves.

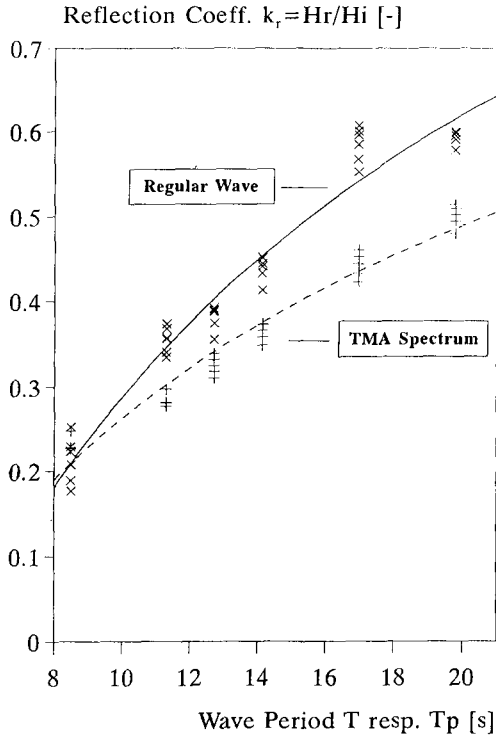


FIG. 7 REFLECTION COEFFICIENT VS. WAVE PERIOD

The reflection coefficient for Accropode armour is also found to be nearly the same as for Tetrapod armour (Fig.8). The large scatter shown in Fig.8 also indicates that the surf similarity parameter does not represent an optimal mean for the description of the reflection process.

**Dissipation and Transmission Coefficients**

Wave-induced pressures have also been measured along the outer slope (seaward), so that the inflow boundary conditions may be described by both pressure (dynamic) and surface elevation (static).

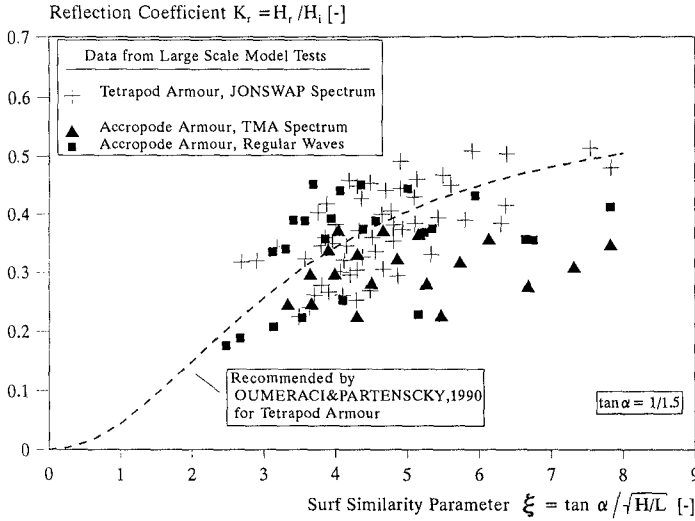


FIG. 8 REFLECTION COEFFICIENT VS. SURF SIMILARITY PARAMETER

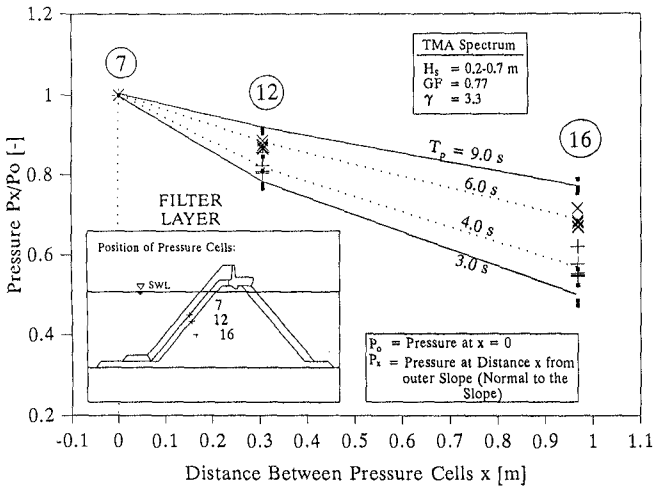


FIG. 9 PRESSURE DISSIPATION WITHIN THE FIRST LAYERS (LOWER ELEVATION, FAR FROM SWL)

The damping rates of the wave-induced pressure in a direction normal to the outer slope is plotted for different wave parameters. The related pressure gradients are evaluated as a function of the wave height, wave period and wave steepness.

Fig.9 illustrates for instance how the dynamic pressures are damped along the line through the locations of the pressure cells 7, 12 and 16. The pressure dissipation in the underlayer is a little higher than that inside the core. The damping rate is related to the wave period. At shorter wave periods ( $T=3.0$  s), the damping in the first layer is about 2.5 times higher than at longer periods ( $T=9.0$  s). Inside the core, however, it is only about 1.75 times higher. Comparing the damping along the line through the pressure gauges 8, 13, 17 and 19 (Fig.10) and along the line through the gauges 7, 12 and 16 (Fig.9) it can be seen that there is a slight increase of the damping rate for all wave conditions when the location of the line considered becomes closer to still water level (turbulent zone).

By considering a direction normal to the outer slope, the pressure gradients within the armour layers may reach values which are more than twice of those in the underlayer and more than four times of those in the first layers of the core material.

By assuming that the wave energy is proportional to the squared wave height ( $E \sim H^2$ ), the reflected, dissipated and transmitted wave energy components are analysed according to Eqs.(1)&(3) and as a function of the incident wave parameters. For this analysis the data recorded by wave gauges and wave run-up gauges has been used.

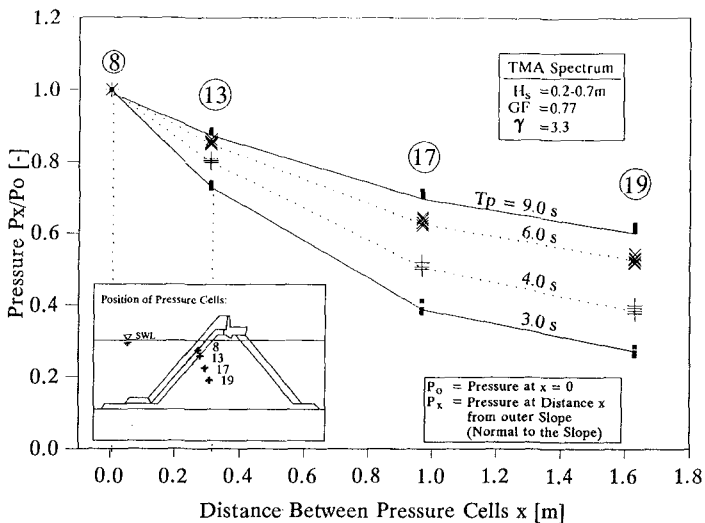


FIG.10 PRESSURE DISSIPATION WITHIN THE FIRST LAYERS (HIGHER ELEVATION, CLOSE TO SWL)

For instance, the results in Fig.11 illustrate the variation of the various energy components as a function of the wave period  $T_p$  for irregular waves with significant wave heights  $H_s=0.2-0.7m$ . The wave parameters in Fig.11 correspond to wave conditions in the Large Wave Flume (GWK). As expected, the reflected and transmitted part of the wave energy increases with increasing wave period while the dissipated energy decreases. In order to better examine the variation of the different components of the dissipated energy described by Eq.(3), Fig.12 has been prepared. It shows in more detail the variation of the dissipated energy in the armour layer, in the filter layer and in the core material as a function of wave period  $T_p$  and for the same wave conditions as in Fig.11. It is seen that the effect of the wave period on the wave energy dissipation is stronger in the outer layers and that in the core material almost no effect can be identified.

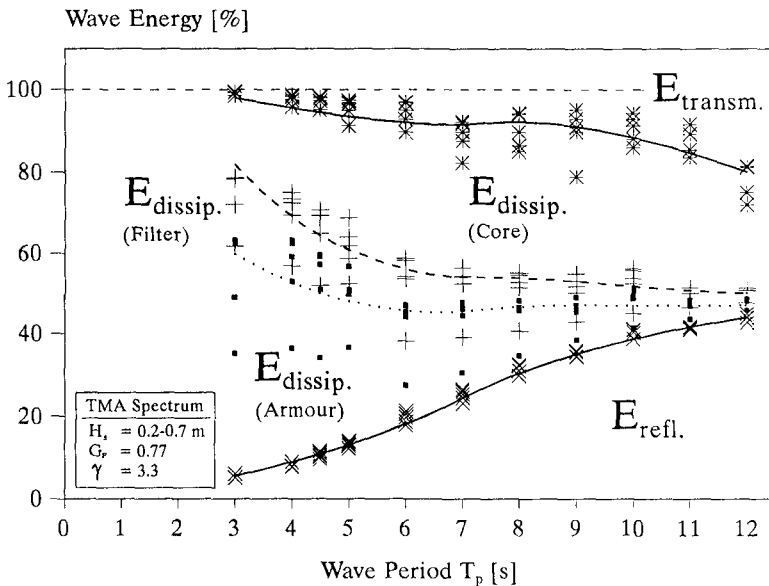


FIG. 11 WAVE ENERGY COMPONENTS VS. WAVE PERIOD

**Concluding Remarks**

The knowledge of reflected waves is determinant for the evaluation of the further dissipated and transmitted wave energy components. Therefore, particular attention has been devoted to the separation of the reflected waves from the measured partial standing wave system. This problem is, however, not definitely solved and the evaluation of reflected waves still remains an estimate.

A further topic which has been particularly dealt with, is the interaction of the wave motion outside the structure and the internal wave-motion. The results which have been reached so far, are expected to contribute to the better understanding of

the coupling mechanisms between external and internal flow which can generally not be satisfactorily described by small-scale model simulation and by existing numerical codes (WIBBELER & OUMERACI, 1992).

The attenuation of wave height and wave-induced pressure in the direction of wave propagation inside the structure is very fast within the first layers. The rate of attenuation tends to strongly increase with increasing wave height.

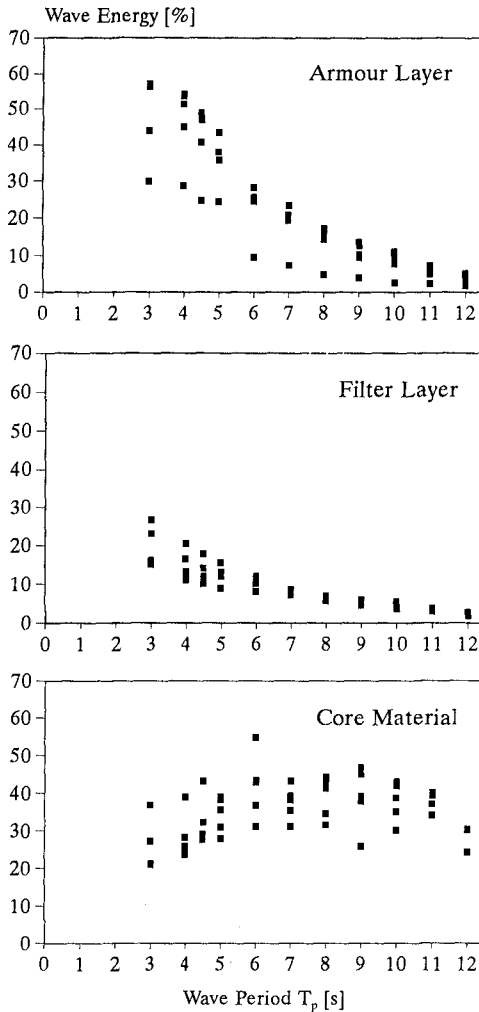


FIG. 12 WAVE ENERGY DISSIPATION IN DIFFERENT LAYERS VS. WAVE PERIOD

As expected, less wave energy is dissipated by a single armour layer (Accropodes) than by a double armour layer (Tetrapods). Consequently, more wave energy has to be dissipated within the underlayer of the Accropode armour than within the underlayer of the Tetrapod armour; i.e. particular effort should be devoted to the design of the underlayer when a single armour layer is used.

It is hoped that the results presented in this paper will eventually contribute :

- (a) to get a better insight into the geohydrodynamic processes affecting the overall stability of the structure as well as the stability of the armour units and further structure components;
- (b) to improve the description of the wave-induced flow on and in the structure and thus to evaluate properly the actual forces on the armour units and further elements of the structures;
- (c) to improve the commonly used simulation tools (small-scale models and numerical codes) by providing reliable data for their validation.

Further research is directed to developing a theoretical method for the approximate evaluation of the dissipated wave energy components in the structure as a function of the wave parameters and the hydraulic properties of the porous media.

### **Acknowledgements**

This study is supported by the German Research Council (DFG), Bonn. It is part of a research programme on breakwaters within the Coastal Engineering Research Unit (SFB 205) at the University of Hannover, Germany.

### **References**

- MANSARD, E.P.D.; FUNKE, E.R.: On the Reflection Analysis of Irregular Waves, National Research Council Canada, Hydr. Labor., Techn. Rep. TR.-HY 011, Ottawa, Canada, 1987.
- OUMERACI, H.; PARTENSCKY, H.W.: Wave-Induced Pore Pressure in Rubble Mound Breakwaters. ASCE, 22nd ICCE'90, Delft, The Netherlands, 1990.
- WIBBELER, H.; OUMERACI, H.: Finite Element Simulation of Wave-Induced Internal Flow in Rubble Mound Structures. ASCE, submitted to 23rd ICCE'92, Venice, Italy 1992.